ELSEVIER

Journal of Food Engineering 61 (2004) 67–81

JOURNAL OF FOOD ENGINEERING

www.elsevier.com/locate/jfoodeng

Development of hyperspectral imaging technique for the detection of apple surface defects and contaminations

Patrick M. Mehl [a], Yud-Ren Chen [b,*], Moon S. Kim [b], Diane E. Chan [b]

[a] *Biomagnetics Group, Vitreous State Laboratory, The Catholic University of America, Hannan Hall, Room 410, Washington, DC 20064, USA*
[b] *Instrumentation and Sensing Laboratory, USDA, ARS, BA, ANRI, ISL, Building 303 BARC-East, 10300 Baltimore Avenue, Beltsville, MD 20705-2350, USA*

Received 26 April 2002; accepted 31 March 2003

Abstract

A high spatial resolution (0.5–1.0 mm) hyperspectral imaging system is presented as a tool for selecting better multispectral methods to detect defective and contaminated foods and agricultural products. Examples of direct linear or non-linear analysis of the spectral bands of hyperspectral images that resulted in more efficient multispectral imaging techniques are given. Various image analysis methods for the detection of defects and/or contaminations on the surfaces of Red Delicious, Golden Delicious, Gala, and Fuji apples are compared. Surface defects/contaminations studied include side rots, bruises, flyspecks, scabs and molds, fungal diseases (such as black pox), and soil contaminations. Differences in spectral responses within the 430–900 nm spectral range are analyzed using monochromatic images and second difference analysis methods for sorting wholesome and contaminated apples. An asymmetric second difference method using a chlorophyll absorption waveband at 685 nm and two bands in the near-infrared region is shown to provide excellent detection of the defective/contaminated portions of apples, independent of the apple color and cultivar. Simple and requiring less computation than other methods such as principal component analysis, the asymmetric second difference method can be easily implemented as a multispectral imaging technique.
Published by Elsevier Ltd.

Keywords: Multispectral; Spectroscopy; Apples; Inspection; Sorting; Food safety; Principal component; Symmetric second difference; Asymmetric second difference; Image processing; Chlorophyll absorption band

1. Introduction

Reports of food-borne illness are increasing in the US due to the high processing volume of food products. With increasing public awareness, food safety has become a primary concern of the US government with the initiative of a multi-agency program aiming to prevent food contamination at the pre- or post-harvest processing stages.

Apples are an important agricultural commodity in the US market. Raw (unpasteurized) apple juice/cider, a major beverage for children in the US, has been identified as a repeated source of *E. coli* O157:H7 contamination, which has caused illness and deaths (CDC, 1996, 1997). One reason that apples can be contaminated with pathogenic *E. coli* is because they may have contacted the ground, which may be contaminated with animal fecal material or ingesta of an animal's gastrointestinal tracts. The animal fecal material or ingesta are reservoirs of pathogenic *E. coli*. The apple juice industry may use these apples for making cider/juice. The pathogenic bacteria may also be passed to apples from bites on the apples by an animal that has pathogenic bacteria in its mouth. Apples with diseased or fungal-contaminated surfaces, and open skin cuts and bruises may become sites for decay and bacterial growth. Developing detection technologies for apple defects and contaminations in the post-harvest preprocessing stage is therefore important for quality and especially for safety.

Apple treatments involving chemical or radiation exposure may be associated with concerns regarding on-line monitoring or verification for safety and effectiveness. For example, drug-resistant human pathogens may develop, leading to the need for changes in the procedures addressing contamination or pathogens on food

* Corresponding author. Tel.: +1-301-504-8450; fax: +1-301-504-9466.
E-mail address: cheny@ba.ars.usda.gov (Y.-R. Chen).

0260-8774/$ - see front matter Published by Elsevier Ltd.
doi:10.1016/S0260-8774(03)00188-2

products (Bergogne-Berezin et al., 1998; CDC, 1998; Cody et al., 1999). Preventive crop protection may use approaches such as pesticides (Garey & Wolff, 1998) that could in turn pose dangers to human health through accumulative residual doses. Less aggressive methods such as atmospheric oxygen reduction (Amanatidou, Smid, & Gorris, 1999) may also need more controls on a continuous basis. Detection of either pathogenic or chemical food contamination is therefore essential. Detection methods are being actively developed using various means such as biosensor devices, diagnostic devices, imaging or spectroscopic devices, and a variety of combined techniques to insure public safety.

Imaging techniques have been developed as an inspection tool for quality and safety assessment of a variety of agricultural food products. Imaging is generally non-destructive, reliable, and rapid, depending on the specific technique used. These techniques have been successfully applied to fruit (Abbott, Lu, Upchurch, & Stroshine, 1997), meat (Swatland, 1995), poultry (Park, Chen, & Nguyen, 1998), and grain (Liao, Reid, Paulsen, & Ni, 1992).

Spectroscopic methods provide detailed fingerprints of the biological sample to be analyzed using physical characteristics of the interaction between electromagnetic radiation and the sample material, such as reflectance, transmittance, absorbance, phosphorescence, fluorescence, and radioactive decay. The analytic spectral regions include the ultraviolet, near-, mid-, and far-infrared regions. The near-infrared (NIR) region in particular has been successfully used for food quality and food safety analysis during the past two decades (Williams & Norris, 1987; Chen, 1992; Chen, Park, Huffman, & Nguyen, 1998; Osborne, Fearn, & Hindle, 1993). Spectrometric studies in the NIR region demonstrated possible use for identifying bruises on apple surfaces (Upchurch, Affeldt, Hruschka, Norris, & Throop, 1990). A more recent study extended the application to identify a wider range of apple surface defects utilizing filtered imaging techniques (Aneshansley, Upchurch, & Throop, 1997). The corresponding statistical analysis showed good surface defect classification at 540, 750, 970 and 1033 nm depending on the apple cultivar and type of defect (Aneshansley et al., 1997). However, the methods are limited in spatial analysis capability.

The multispectral imaging technique combines analysis of both spatial and spectral characteristics of a sample. A discrete number of wavelengths (up to six for most systems) are selected using filters in the machine vision system to reconstruct sample images before proceeding to image processing and analysis (Gat, 1998). However, there are no easy methods for choosing the optimal filter sets for multispectral imaging systems suitable for any given food or agricultural product. In fact, the determination of appropriate filters to use for each apple cultivar has been mostly experimental, which we address in this paper.

Hyperspectral imaging, an emerging technology developed in recent years, can be used as a tool to obtain a few optimal filters for a multispectral imaging system. A hyperspectral imaging system is currently utilized at the Instrumentation and Sensing Laboratory (ISL) for analyzing spectral data of various food products and the possible presence of contaminations. This technique has been presented as combining the advantages of spectroscopy and imaging techniques (Lu & Chen, 1998). This technology is a spectral continuum version of the multispectral technique, with many potential food quality and safety applications (Chen, 1992; Chen et al., 1998). However, the technology thus far is very slow and cannot be implemented in a real-time detection system.

Hyperspectral imaging results in a set of pixels, each with its own continuous spectrum. The set of pixel intensities at a particular wavelength of the spectrum represents a gray scale image of the sample at that wavelength. Two acquisition methods are available: (1) a series of full spatial images at each of the given wavelengths (or narrow bands) is recorded, i.e., liquid crystal tunable filter (Gat, 1998), or (2) a series of spatial lines are scanned across the sample with a spectrum recorded at each pixel of the spatial line. This study uses the second approach, as previously described (Lu & Chen, 1998). Two separate technologies exist for that purpose. The first uses a moving camera and slit to scan an immobile sample (Martinsen, Schaare, & Andrews, 1999), and the second uses a stationary camera and slit to scan a moving sample. The second technology is currently used at ISL.

Different approaches for hyperspectral data analysis can be developed and applied, depending on the spectral characteristics presented by the sample material. Two analysis methods are presented, a direct spectral analysis (Aneshansley et al., 1997) and the second difference method (Chen et al., 1998; Hruschka, 1987). An asymmetric second difference method has been developed. The first method uses direct spectral band imaging of the intrinsic spectral characteristics of the sample. For a vegetation product, those spectral characteristics in the visible region are largely due to photosynthetic pigments including chlorophyll and accessory pigments such as carotenoids. The specific absorption peak for chlorophylls (Govindjee, Papageorgiou, & Rabinowitch, 1967) can then be used to detect damage, defects, or contaminations on fruit surfaces. Spectral bands in the NIR region are also used for the determination of surface defects on fruits and vegetables (Abbott et al., 1997). The asymmetric second difference method is presented as a more general approach of the second spectral difference that is not limited to a symmetric approach to

estimate the spectral differences. In this study, the asymmetric method is tested as a means of detecting various defective/contaminated areas on apples.

The objectives of this paper are: (1) to present the development of an improved hyperspectral imaging system currently used at ISL, (2) to demonstrate the capabilities of the hyperspectral imaging system to provide a more complete fundamental analysis leading to the development of faster and more efficient multispectral imaging methods, and (3) to compare the asymmetric second difference method with methods such as principal component analysis (PCA) or symmetric second differences, for the detection of defects and contaminations on the surfaces of various apple cultivars.

2. Materials and methods

2.1. Apples

Red Delicious, Golden Delicious, Gala, and Fuji apples were collected after harvesting and before processing, without any anti-fungal treatment or wax protection. These wholesome apples were obtained either directly from the apple trees or from collection barrels at a Pennsylvania apple grower in (Rice Fruits Company, PA, USA), before any processing treatments or caliber sorting were performed. At the same location, defective and contaminated apples (showing obvious defects or damage) were obtained from the trees or barrels, or picked up from the ground in the apple orchard. Apples collected from the ground were damaged, contaminated, or diseased. The damaged and contaminated apples included those with side rots, bruises, flyspecks, scabs and molds, black pox (a minor fungal disease), and other fungal and soil contaminations. Apples were placed in trays, contained within plastic bags to avoid moisture loss, and boxed for transport. Apples were then stored in an environmental room maintained at a temperature ranging between 0 and 4 °C.

Individual cultivars have their own characteristic size and color. Red and Golden Delicious apples are generally large apples, with occasional small caliber apples. Red Delicious apples present a major red color on the sunny side with a very minor yellowish color on the side hidden from the sun. Golden Delicious apples present a strong golden yellow color with a hint of red on the sunny side. Gala and Fuji apples are smaller, mixed color apples. Gala apples show a red color combined with stripes of orange and yellow, and Fuji apples show a red color combined with stripes of yellow and green. Determination of the chlorophyll absorption spectrum for each of the cultivars was performed on both sunny and hidden sides to support our analysis.

2.2. Hyperspectral imaging system

Fig. 1 is a schematic diagram of the ISL hyperspectral imaging system. It consists of a charge coupled device (CCD) camera system SpectraVideo™ Camera from PixelVision, Inc. (Tigard, OR, USA) equipped with an imaging spectrograph SPECIM ImSpector version 1.7 from Spectral Imaging Ltd. (Oulu, Finland). The ImSpector has a fixed-size internal slit to define the field of view for the spatial line and a prism/grating/prism system for the separation of the spectra along the spatial line.

To improve the spatial resolution of the hyperspectral images, an external adjustable slit is placed between the sample and the camera optical set. This better defines the field of view and increases the spatial resolution.

The image acquisition and recording is performed with a Pentium-based PC using a general purpose imaging software, PixelView™ 3.10 Beta 4.0 from PixelVision, Inc. (Tigard, OR, USA.). A C-mount set with a focus lens and an aperture diaphragm allows for focusing and aperture adjustments, for which the circular aperture is opened to its maximum and the external slit is adjusted with micrometer actuators to optimize light flow and resolution.

The light source consists of two 21 V, 150 W halogen lamps powered with a regulated DC voltage power supply from Fiber-Lite A-240P from Dolan-Jenner Industries, Inc. (Lawrence, MA, USA). The light is transmitted through two optical fibers towards a line light reflector. The sample is placed on a conveyor belt with an adjustable speed AC motor control Speedmaster from Leeson Electric Motors (Denver, CO, USA).

The sample is scanned line by line with an adjustable scanning rate, illuminated by the two line sources as it passes through the camera's field of view. A more complete description of the system is presented in a companion paper (Kim, Chen, & Mehl, 2001).

2.2.1. Spectral calibration

A set of Hg–Ne, Ne, A, Kr pencil lights from Oriel Instruments (Stratford, CT, USA) was used for the spectral calibration of the hyperspectral imaging system. The spectral range was found to be 424–899 nm. The camera offers a 256-pixel range for the spectral line. A 128-channel range was used with a 2-binning process along the spectral line in this study. With a correlation coefficient of $R^2 = 0.9983$, wavelength is correlated to pixel number p by the following spectral calibration equation,

$$\lambda_p = 3.6763p + 420.87 \text{ nm} \quad (1)$$

where λ_p is the wavelength at pixel p. Spectral resolution is determined per pixel of the spectral range for the system. The Hg–Ne lamp is also used for the spectral alignment of the ImSpector (Prism/Gratings/Prism) with

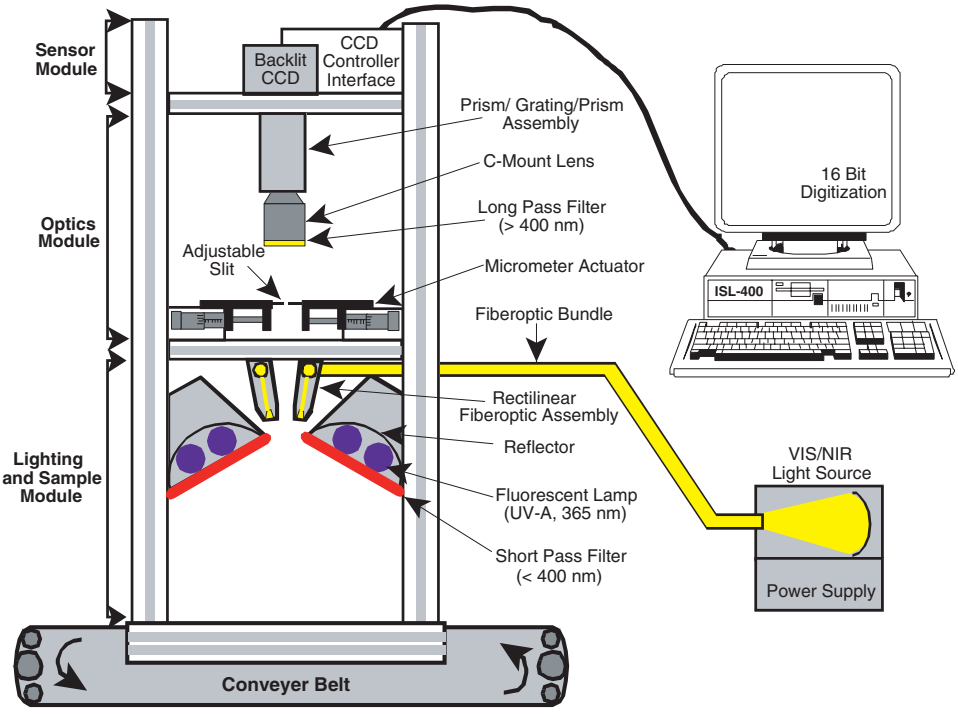

Fig. 1. Schematic of the hyperspectral imaging system.

the CCD camera. The variation of the spectral band along the spatial line is between 1 and 2 pixels, corresponding to a shift of less than 6 nm.

2.2.2. Spatial resolution

A 2-in. square standard US Airforce 1951 resolution grid, purchased from Edmund Scientific Co. (Tonawanda, NY, USA) was used to determine the spatial resolution along the X and Y axes (the acquisition line and the scanning axis, respectively). Also from Edmund Scientific Co. was a square complementary distortion grid with sets of circular points with respective diameters of 1, 0.75 and 0.5 mm and separated by 1, 0.75 and 0.5 mm, respectively. This grid was used to determine the existence of any distortion at the edges of the field of view and also to check the spatial resolution of dots. The spatial resolution was found to be between 0.75 and 0.5 mm along the X and Y axes. It was observed that the resolution decreases with increasing wavelengths. The distortion is slightly increased on the edges of the spatial lines within the level of 0.5–0.75 mm resolution.

2.2.3. Imaging acquisition methods

The spectral line acquisition was performed at a room temperature of 20 °C. Wholesome apples were chosen randomly, while defective/contaminated apples were selected for identifiable defects or contaminations. The exposure and acquisition time was set between 15 and 50 ms for reflectance. The scanning frequency was determined according to the rate of line acquisition to preserve the proper spatial aspect ratio.

The sample trays were painted with flat black paint to minimize background reflectance. The CCD camera dark current and near-100% reflectance of a white reference panel (Spectralon™ by Labsphere, North Sutton, NH, USA) were recorded before proceeding to the acquisition of the hyperspectral images of the apples.

Raw reflected light intensities from the samples were recorded line by line during the scanning of the samples. After corrections for dark current at each pixel, monochromatic images were converted into percent reflectance using either the commercial software package ENVI 3.2 from Research Systems, Inc. (Boulder, CO, USA) or in-house software. These monochromatic images were then assembled and formatted as ENVI files for further analysis.

2.2.4. Analysis methods

2.2.4.1. Direct monochromatic observation. Direct visual observation of the apples is usually sufficient for inspectors to sort wholesome from contaminated apples. It is therefore logical to find specific wavelengths at which defects/contaminations are well contrasted from normal apple areas. A threshold method can then be used to classify the apples. The observations from this study will be compared with the conclusions reported by Aneshansley et al. (1997) for their considered wavebands. Also, the selected spectral ranges to be used for

second difference methods are based on these direct spectral observations.

2.2.4.2. Second difference method. The second difference technique is based on a wider analysis of the spectral characteristics from 400 to 900 nm. Direct observations of the symmetric second spectral differences are used for image analysis.

2.2.4.2.1. Second difference—symmetric model. Each spectrum at each pixel of the image is compared for the normal and contaminated apples. An in-house software package is used for determination of the second differences of the spectra, particularly in the red region of the chlorophyll *a* absorption band. This method was previously applied with success for food safety inspection of chickens, to preprocess spectral input data to neural networks used to classify wholesome and unwholesome chickens (Chen et al., 1998; Hruschka, 1987). In general, using second differences is a common method in the area of NIR spectroscopy. The algebraic expression of the second central difference is given by the following equation:

$$S''(\lambda_n, g) = S(\lambda_n + 3.6763g) - 2S(\lambda_n) + S(\lambda_n - 3.6763g) \quad (2)$$

where $S(\lambda_n)$ is the reflectance at point n, $S''(\lambda_n, g)$ is the second difference value of the spectrum at the wavelength λ_n, and g is the gap factor between spectral points (3.6763 nm between spectral points according to the spectral calibration performed). The principle of this method is a discrete determination of the presence of a weak or strong absorption peak of the spectrum at the wavelength λ_n. The optimal gap size is an indication of the wideness of the peak, and the gap value g is optimized to provide the highest contrast between normal and defective/contaminated apple sites. This value depends on the spectral range in consideration and on the apple cultivar. One advantage of this method is the reduction of the background contribution.

2.2.4.2.2. Second difference—asymmetric model. The symmetric model can be generalized to an asymmetric formulation,

$$S''_b(\lambda_n, g_1, g_2) = [g_1 S(\lambda_n - 3.6763g_1) - (g_1 + g_2)S(\lambda_n) + g_2 S(\lambda_n + 3.6763g_2)]/(g_1 + g_2) \quad (3)$$

with the same notations as for (1), and where g_1 and g_2 are, respectively, the left and right gap factors. $S''_b(\lambda_n, g_1, g_2)$ is the difference between the intensity signal $S(\lambda_n)$ and the estimated signal intensity of the points $\lambda_n - 3.6763g_1$ and $\lambda_n + 3.6763g_2$. This expression provides a greater freedom of choice for comparing important spectral bands.

2.2.4.3. Principal component analysis. This study uses the ENVI software package for the application of PCA to the hyperspectral images of the apples. The principle of the analysis is the following: having initially a vector basis (wavelengths) describing the image, a correlation matrix between each initial vector is determined. Linear combinations of these vectors are then determined to provide a new rotated vector basis as an ordered set of orthogonal (uncorrelated) vectors with the order of this orthogonal vector basis being defined by decreasing contribution of the uncorrelated vectors to the reconstruction of the image. In other words, the associated eigenvalues to the eigenvectors of the correlation matrix are calculated and ordered in a decreasing value order. This method allows for a reduction of contributing vectors, or factors, describing the image as performed for the factor analysis technique in multivariate analysis. The methodology for the algorithm can be found in Malinowski and Howery (1980).

In order to apply the PCA method, preliminary masking of the apples and selection of the wholesome apples are performed. PCA is then applied to these masked apples in the spectral range of 682–900 nm to select the most significantly contributing linear wavelength combinations or PCA bands. The original hyperspectral image with the good and bad apples is then rotated along these PCA bands to calculate the loadings, or ''scores'', for each pixel of the image along the considered PCA axis (Richards, 1994). The scoring provides the gray scale of each image pixel leading to a possible classification of good and defective/contaminated areas on the apples. The spectral contribution for each principal component is also determined using the coordinates of the corresponding eigenvectors for further analysis of the spectral ranges contributing most to the best detection.

3. Results and discussion

Fig. 2 shows the RGB color images of five intact and five contaminated apples for each of the four cultivars: (a) Red Delicious, (b) Golden Delicious, (c) Gala, and (d) Fuji apples, taken using a digital camera. The defective/contaminated apples exhibited soil contamination, bruising, fungal growth (Sooty Blotch), and disease (Black Pox). Representative spectra from wholesome and defective/contaminated spots on individual cultivars are shown in Fig. 3 for (a) Red Delicious, (b) Golden Delicious, (c) Gala, and (d) Fuji apples.

Fig. 3a–d show that, in general, normal (wholesome) apple surfaces have higher reflectance in the Vis and NIR region than the defective/contaminated surfaces have. Two exceptions to this were for bruised spots, and for soil contamination on red delicious apples in the 450–550 nm region. Among the types of defective/contaminated areas, bruises have higher reflectance than the others, and scab areas have the lowest reflectance. There

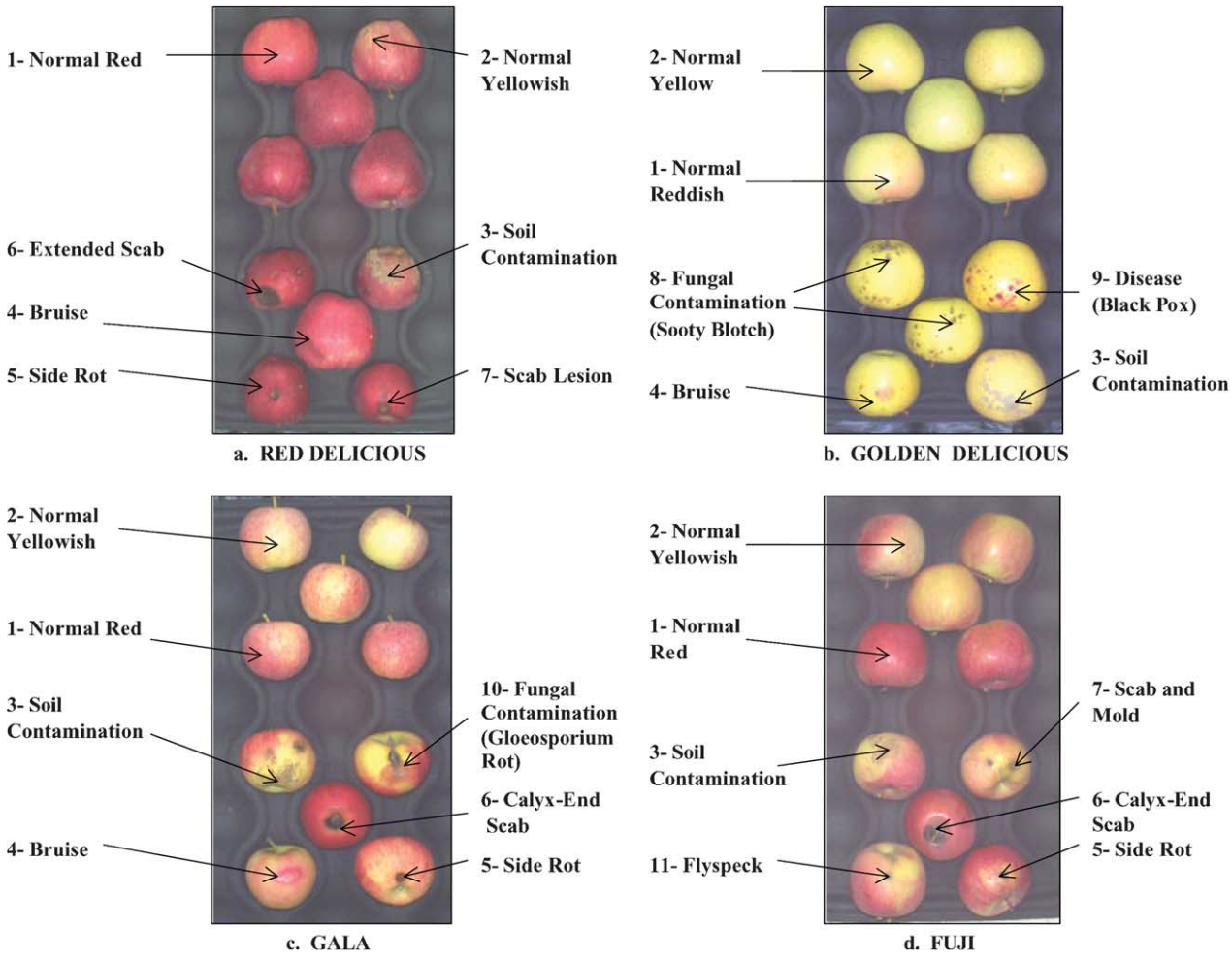

Fig. 2. RGB color images of apple cultivars: (a) Red Delicious, (b) Golden Delicious, (c) Gala, and (d) Fuji. The five top apples are normal and the five bottom apples are damaged or contaminated.

is a very distinct absorption at 682–684 nm (chlorophyll *a*) for normal and bruised areas. Areas with Black Pox and Sooty Blotch showed some chlorophyll *a* absorption, while other infected areas have almost no absorption at the same band. A low reflectance (or high absorbance) appears in the 450–550 nm carotenoid absorption region even for defective/contaminated apple areas. Direct observation of these absorption variations is difficult and may only be seen using the second difference methods.

3.1. Direct monochromatic observation

Monochromatic images at the 542, 682, and 752 nm spectral bands for each cultivar are given in Fig. 4. Aneshansley et al. (1997) found that wavebands corresponding to 542 and 752 nm give a greater statistical difference between surface defects and normal parts of apples. Golden Delicious apples were the only apples in this study to have a relatively homogeneous skin color. Consequently, they are the only ones with observable surface defects at 542 nm. For the other cultivars, the color variations interfere with a possible threshold setting for the classification of surface defects. Various defects and contaminations are visible in varying degrees at longer wavebands. However, there are no single waveband images that can be used easily to differentiate normal apples from all apples that are either defective or contaminated. For the images at the chlorophyll *a* absorption band of 682 nm, the bruised areas are not easily differentiable from the normal apples. Similarly, at 752 nm, the bruised apples have the same appearance as the normal apples.

3.2. Second difference method

3.2.1. Symmetric second difference

Symmetric second difference images for the four apple cultivars using either the chlorophyll band or the pigment bands are given in Fig. 5. For the second dif-

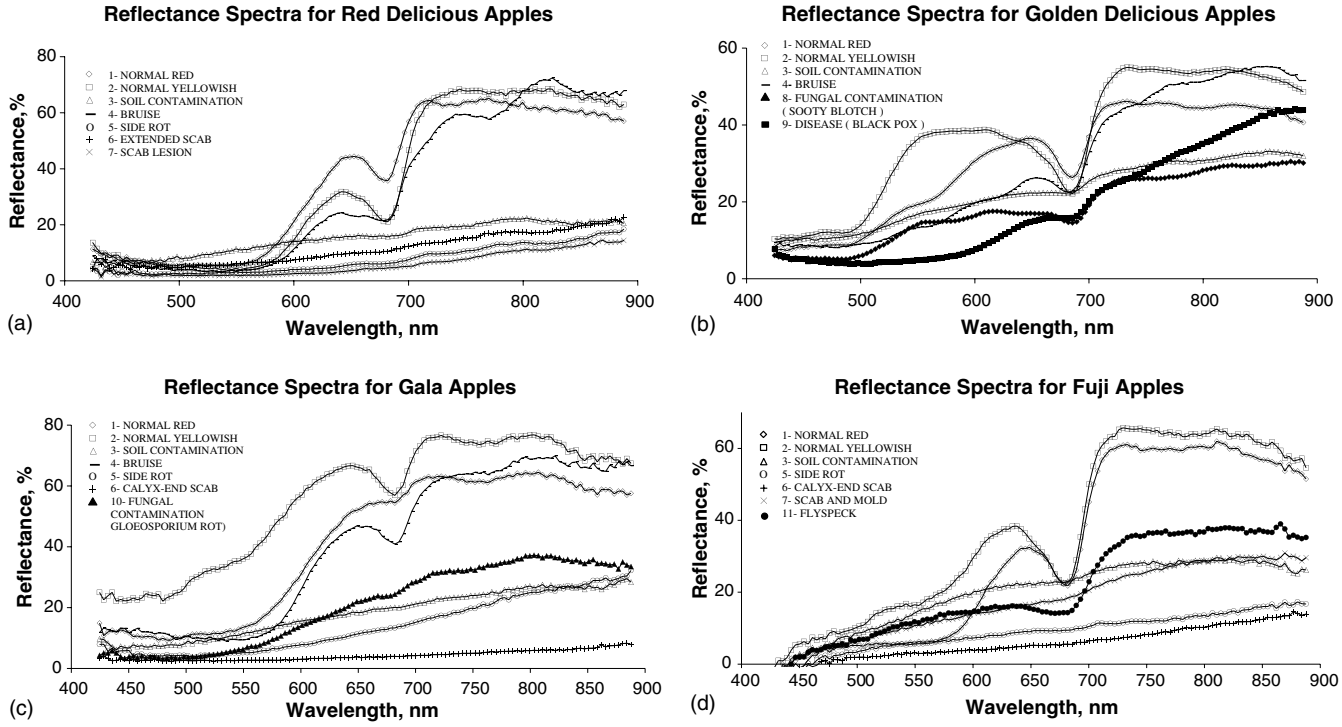

Fig. 3. Reflectance spectra measured by the hyperspectral imaging system for features on (a) Red Delicious, (b) Golden Delicious, (c) Gala, and (d) Fuji apples, corresponding to the numbered spots in Fig. 2.

ference images in each figure, the five normal apples are in the upper portion and the 5 contaminated apples are shown in the lower portion of each image. It should be noted that the second difference reverses the contrast of the samples and the tray background at the 686 nm.

The center wavelength and the gap value g are selected to provide the best contrast between surface defects and normal parts of the apples. At the left side of the figures are the second difference images in the pigment region. For example, for Gala apples, the center waveband is taken at 527 nm. With $g = 11$, the left waveband is at 486 nm, while the right waveband at 567.5 nm. For Golden Delicious apples, the center waveband is taken at 450 nm. With $g = 7$, the left waveband is at 424 nm, while the right waveband is at 476 nm.

In general, the contaminated portions of apples are very distinct and visible for all cultivars. Unfortunately, a majority of the normal apples also present features similar to the contaminated apples, with the exception of Golden Delicious apples. For the Golden Delicious apples, the images are relatively homogeneous at these bands, and the carotenoid absorption band at 450 nm provides good visual separation for fungal contamination (Sooty Blotch), disease (Black Pox), soil contamination, and bruise from the wholesome apples (Fig. 5b). For the other mixed color apples, a large variation of pigment distribution is observed. Application of classification techniques for these complex images of mixed color apples is therefore difficult when using these pigment absorption bands.

In Fig. 5, the center image of each set of three is the second difference image with center waveband at the 675 nm chlorophyll band. With $g = 3$, the left waveband is at 664 nm and the right waveband is at 686 nm. For the Fuji apples, the images of normal apples are uniform, and the contaminations are clearly present. For Golden Delicious, the contaminations are shown as compared to the normal apples, but they are less pronounced than the Fuji apple contaminations. In general, when using the 686 nm chlorophyll absorption band as the edge band for the 675 nm central band, the second differences provide good visual separation of the contaminated parts from the normal parts of the apples, except for the Gala apples. For Red Delicious, the bruised area is not as clearly presented. For the case of Gala, the results are disappointing. The weak chlorophyll absorption combined with the wide variation of colors for the Gala (Fig. 5c) results in a poor resolution for this second difference band.

In Fig. 5, the image on the right in each set of three is the second difference with the center band at the 685 nm chlorophyll absorption band. With $g = 11$, the left waveband is at 645.5 nm and the right waveband at 722.5 nm. Using the 685 nm chlorophyll absorption band as a central band for the second difference method has the advantage of using information from the NIR region and consequently is less color dependent than

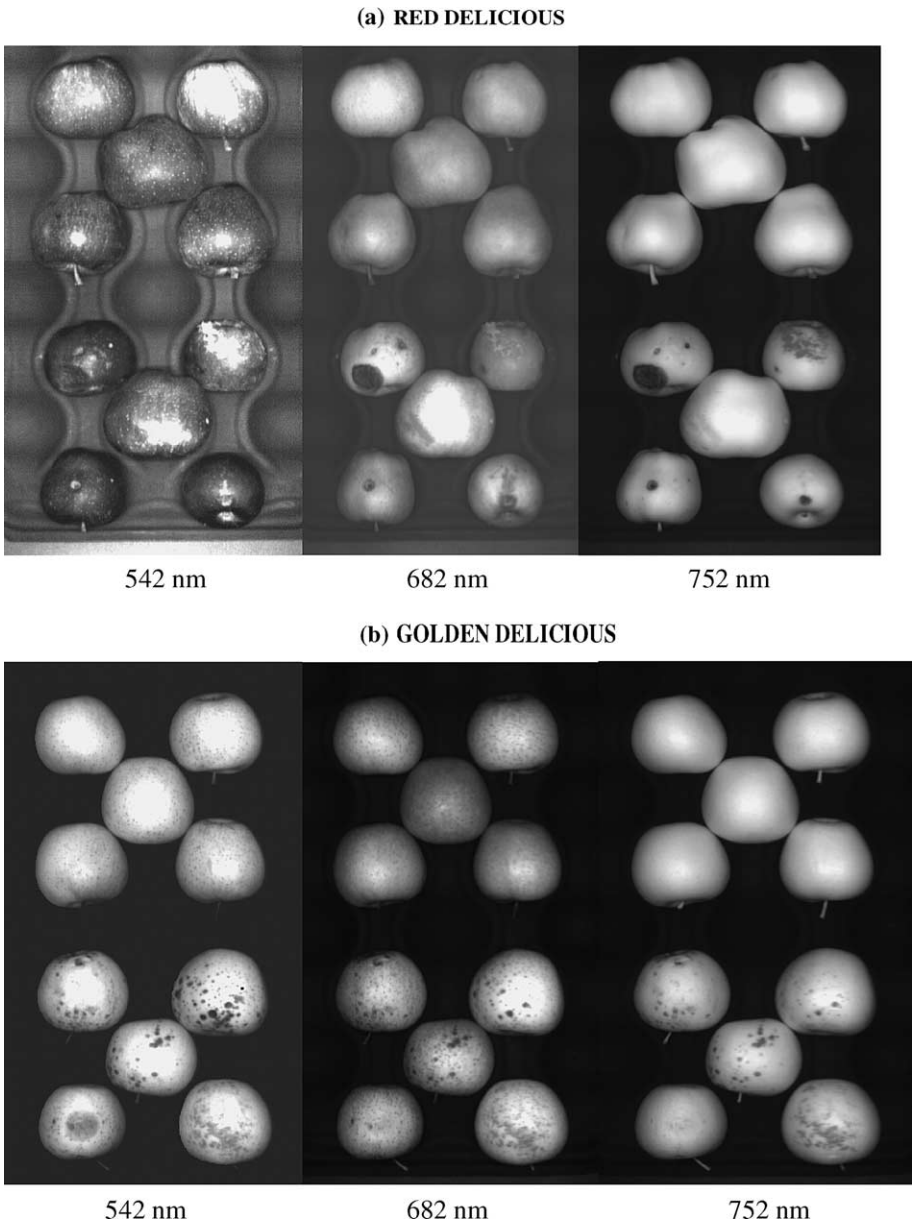

Fig. 4. Monochromatic images at 542, 682, and 752 nm for (a) Red Delicious, (b) Golden Delicious, (c) Gala, and (d) Fuji apples.

using information only from the visible spectral range. As noted previously, the changes in chlorophyll or pigmentation for bruises are not as pronounced in this spectral range as they are in the visible range. The fungal contaminations, soil contaminations, diseases, and scabs are visually separable and the bruises are not clearly visible. For the Gala apples, only the bruise and the rotten part below a scab are not observed, but the other defects are clearly seen.

It is therefore clear that either the 675 or 686 nm band as a center band can be used for the determination of the main contaminations and defects on the four apple cultivars in this study. But the separation of bruised and/or rotten parts from good apple parts for the Gala apple and to a lesser extent for the other apple cultivars cannot be accomplished using the symmetric second difference method.

3.2.2. Asymmetric second difference

We showed that: (1) NIR bands are not subject to color changes from the different apple cultivars, and (2) the red chlorophyll absorption band is a good spectral indicator of good (wholesome) apples. Consequently, the asymmetric second difference method was tested using two NIR bands and the chlorophyll absorption band at 682–686 nm. Fig. 6a–d show the images of the four apple cultivars using $S''_b(\lambda_n, g_1, g_2)$ with $g_1 = 10$, $g_2 = 40$ and $\lambda_n = 722$ nm. These three bands at 685, 722,

(c) GALA

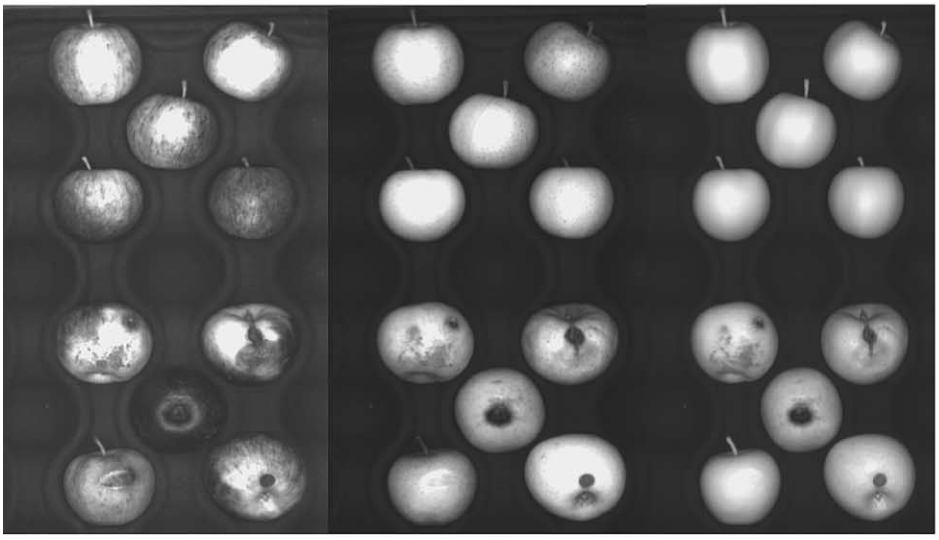

542 nm 682 nm 752 nm

(d) FUJI

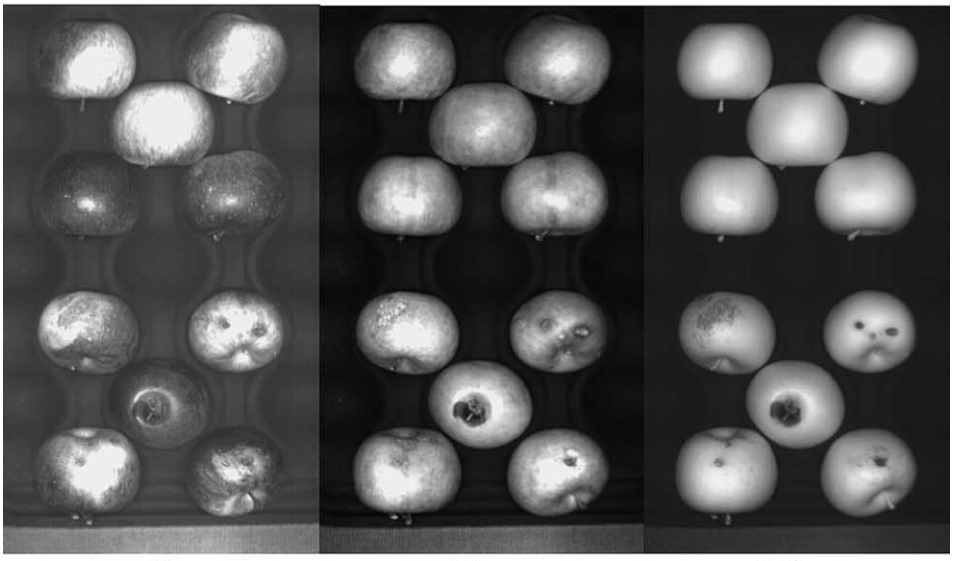

542 nm 682 nm 752 nm

Fig. 4 (*continued*)

and 869 nm are used for the asymmetric second difference. The 722 nm band is that at which the increasing intensities from Vis to NIR start tapering off, and the 869 nm band is an arbitrarily chosen band at the edge of NIR region measurable with the ISL hyperspectral imaging system.

Fig. 6 shows the results of detection of the diseased and contaminated spots on the four cultivars using simple background masking and thresholding image processing techniques. In Fig. 6a–d each of the four apple cultivars has 4 successive images: (1) image at the chlorophyll absorption band, (2) image using the asymmetric second difference, (3) the mask image obtained after morphological processing is applied to image (2), and (4) image of the final result after masking and threshold analysis of the apple set.

Comparison of the asymmetric second difference images in Fig. 6 with the RGB color images in Fig. 2 shows that all the defects and contaminations are visually defined. It was also noted that the stems are not observed as defects but as being parts of good apples. The bruised parts of the apples are apparent and soil contaminations are also very apparent. The diseases, fungal contaminations, and rotten parts are the most

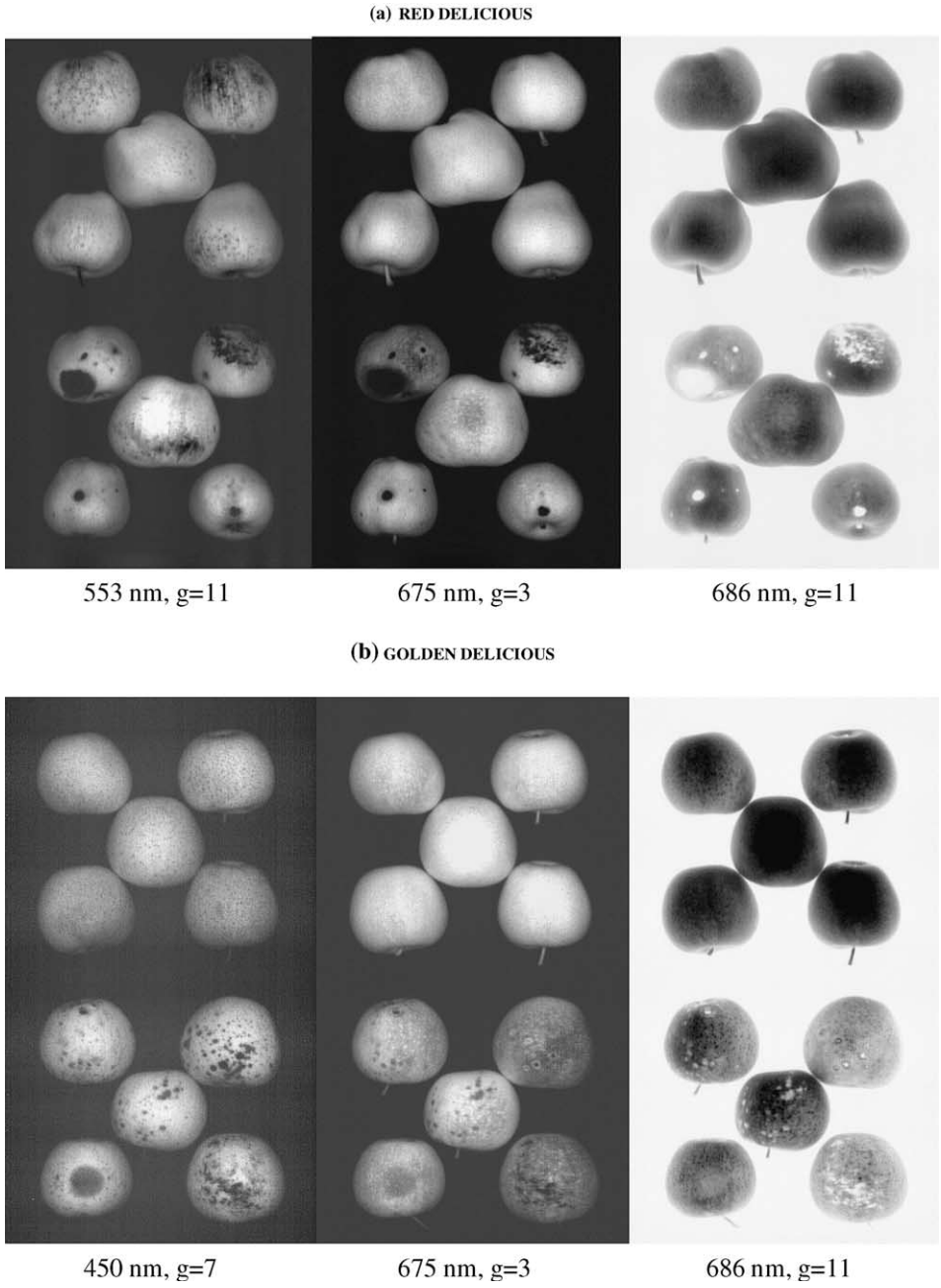

Fig. 5. Symmetric second differences images calculated at different reported wavelengths with the corresponding gap g, for (a) Red Delicious, (b) Golden Delicious, (c) Gala, and (d) Fuji apples.

visible parts on these images compared to the symmetric second differences. One important observation from Fig. 6 is that all four apple cultivars show the same appearance for good apples. There is no difference in the observations of the different apple cultivars using this methodology.

After simple masking and thresholding, defective and contaminated parts can be identified as shown in the far right images in Fig. 6. In these thresholded images, all the diseases and contaminated spots are clearly identified. All the intact apples show no defects or contamination except the one apple positioned at the upper-right corner of the normal Red Delicious apple group. The slight speck shown on the thresholded image is believed to be an actual tiny bruised spot on the otherwise intact, normal apple.

The defective and soil-contaminated spots on the apples are clearly identified and the apples with defects and contaminations can be easily separated from the wholesome, normal apples using the three wavebands for the asymmetric second difference method. Among the defects and contaminations, the bruises have rela-

(c) GALA

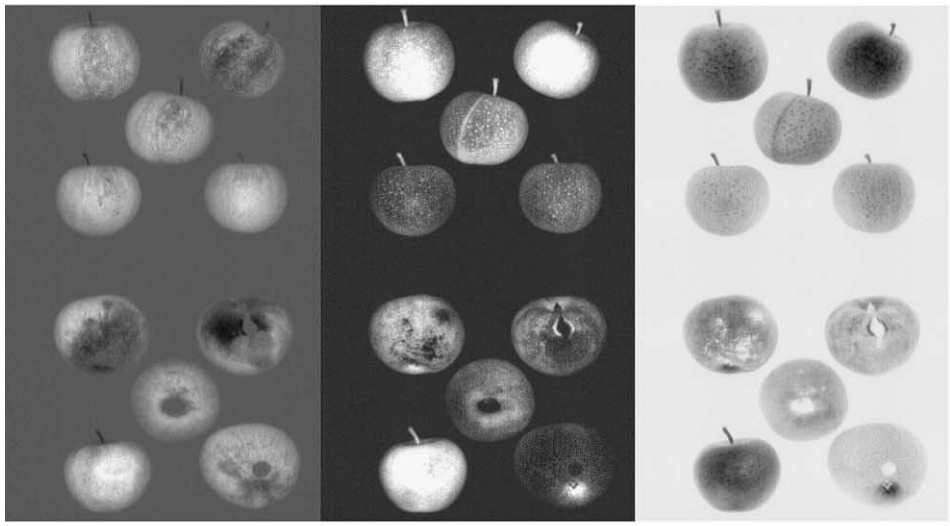

527 nm, g=11 675 nm, g=3 682 nm, g=11

(d) FUJI

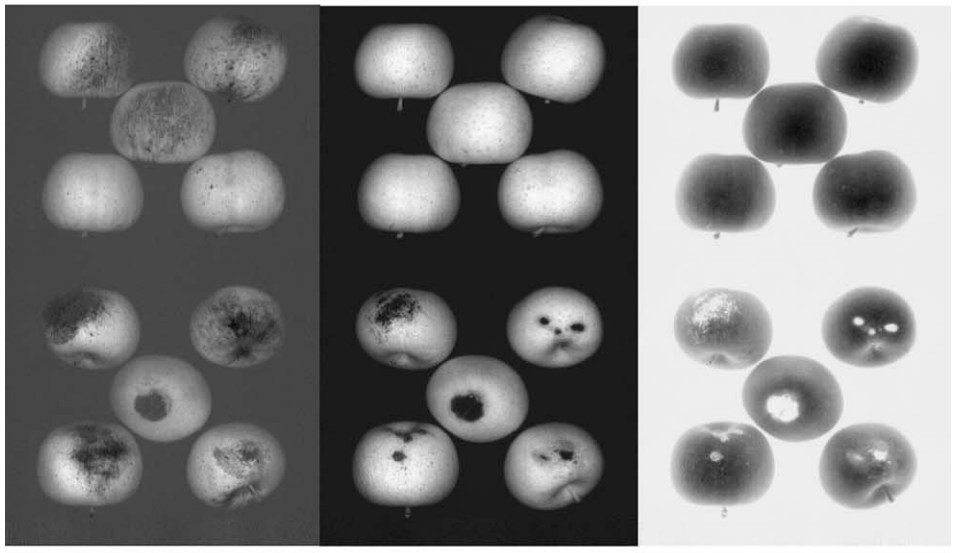

535 nm, g=11 675 nm, g=3 686 nm, g=11

Fig. 5 (*continued*)

tively low contrast with the surrounding portion of the apples than other defects have. Before conducting thresholding for the bruised spots, some simple image processing such as contrast enhancement may be necessary.

3.3. Comparison of PCA and asymmetric second difference

The first PCA band for all the apple cultivars appears to correspond to the average infrared intensity between 750 and 900 nm, as no color features are apparent. Only specific damages and contaminations are visible in the NIR region and bruises are difficult to distinguish using the first principal component. The second principal band is more complex and is associated with the chlorophyll band absorption at 682–700 nm. Specific features and color are more apparent. The third principal component appears to possess characteristics common to all four apple cultivars. This principal component can be used to separate the disease, fungal, and soil contaminations and also the bruises on the bad apples from the good apples. The remaining principal bands provide other details that are not common to the four cultivars. The fourth

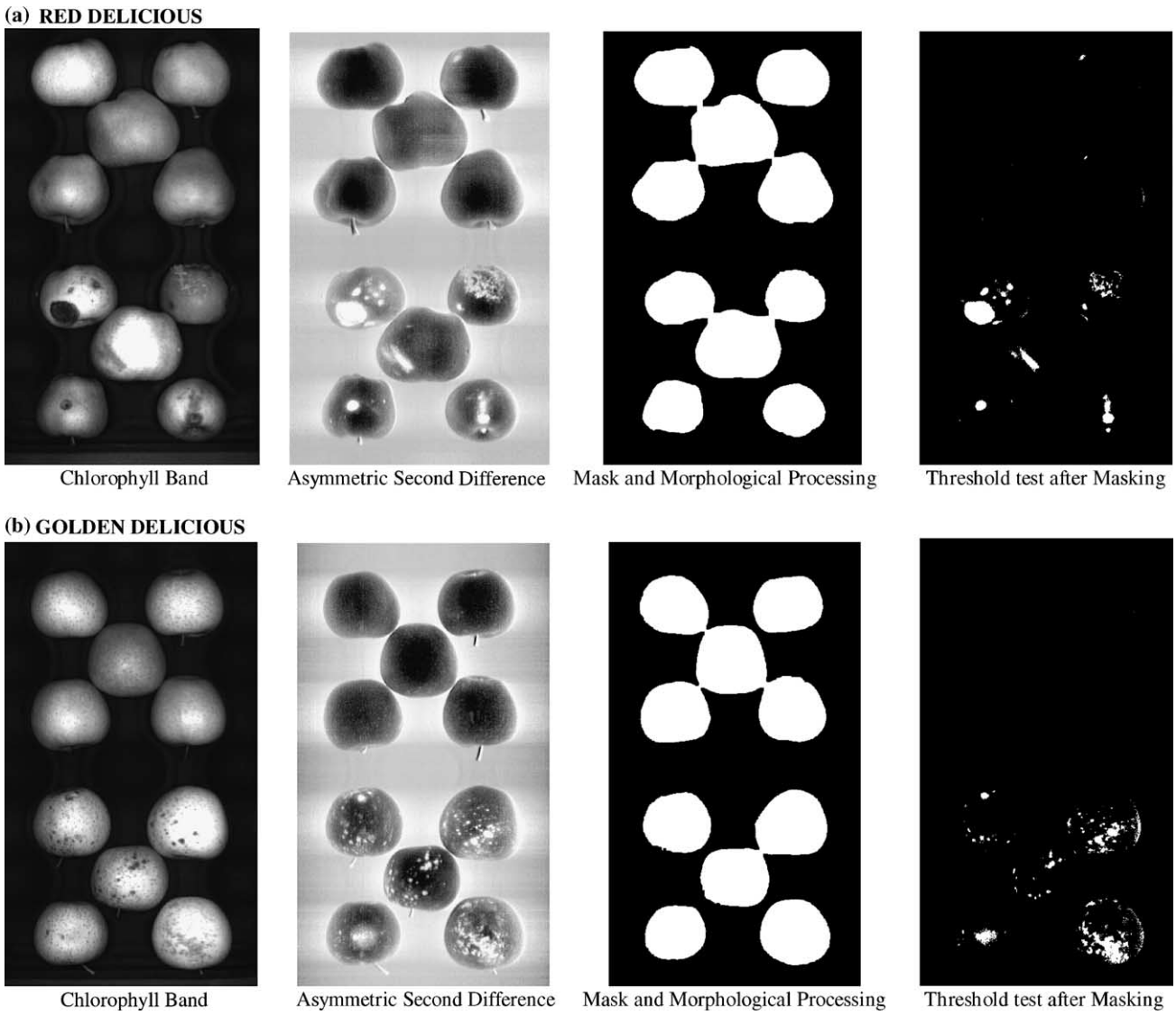

Fig. 6. Asymmetric second differences images calculated at 722 nm with gaps of 10 and 40 for the left and the right wavelengths, respectively (see Section 2), for (a) Red Delicious, (b) Golden Delicious, (c) Gala, and (d) Fuji apples.

principal component could not be easily exploited for classification, as it appears to be dependent on the apple cultivar. The noise level becomes predominant for principal components above 6–10th component, depending on the apple cultivar. Only the first and the third principal bands provide images that are not dependent on the color and shape of the different apple cultivars. The third is chosen because it enhances the contrast between the normal and abnormal portions of the apples. The corresponding spectral contributions for the four apple cultivars are reported in Fig. 7. These spectral range contributions can be used to design a multispectral imaging technology for defect detection. These spectral ranges are similar to those needed for the definition of the most sensitive asymmetric second difference.

The apple images for the four cultivars using the asymmetric second differences method and the third principal band are compared in Fig. 8. These images are visually similar. Diseases, bruises, and contaminations are almost identically visible with perhaps a slightly more defined resolution for the third principle band for the bruises. Better detailed images were obtained by the PCA method for not only contaminated apples but also wholesome ones. This is particularly noticeable for the Golden Delicious apples. Consequently, defects and contaminations are not quite as well highlighted and contrasted using PCA, compared to the asymmetric second difference method. The latter gives less detail to the good apples, and thus a better background from which to distinguish defects and contaminations.

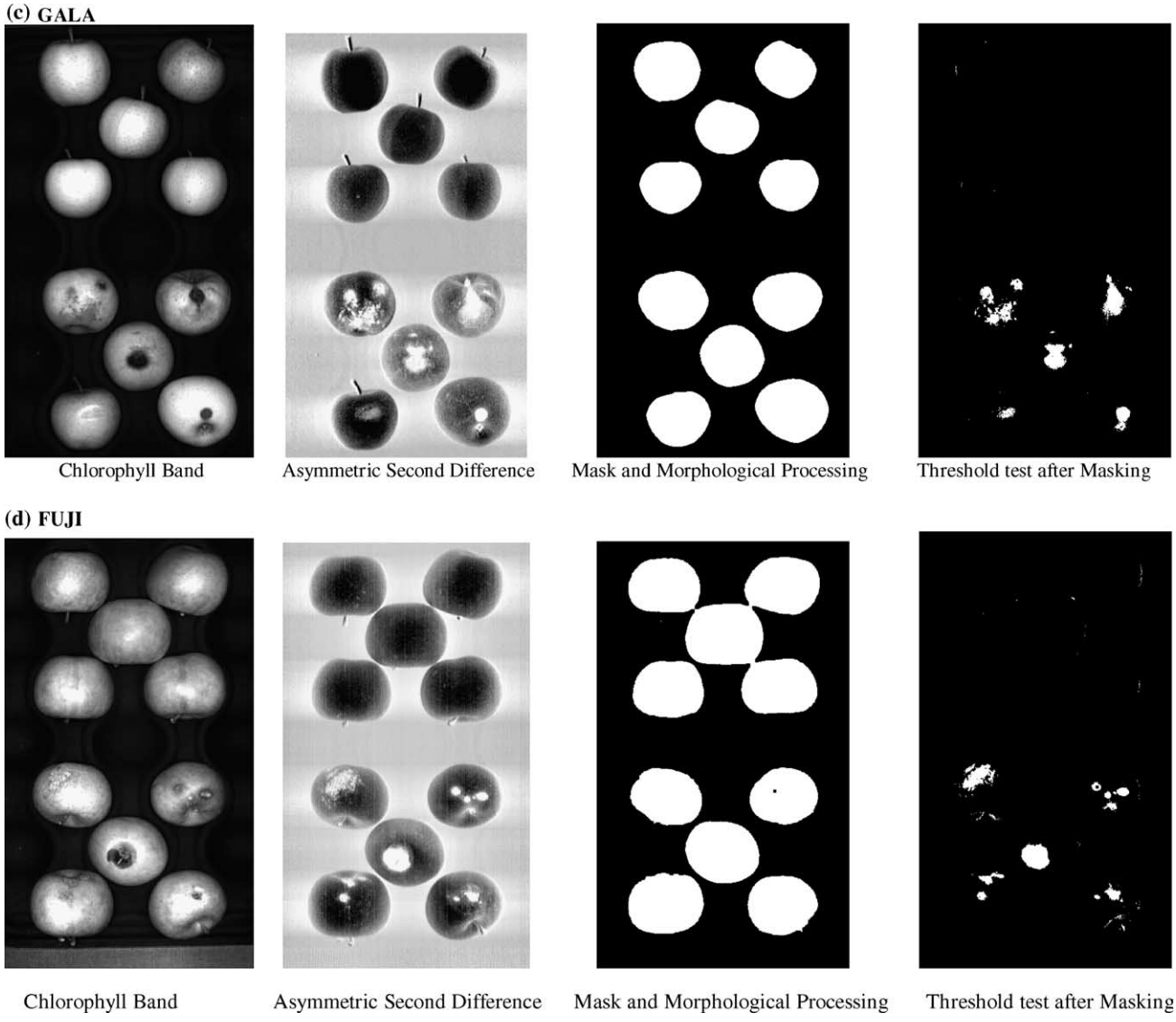

Fig. 6 (*continued*)

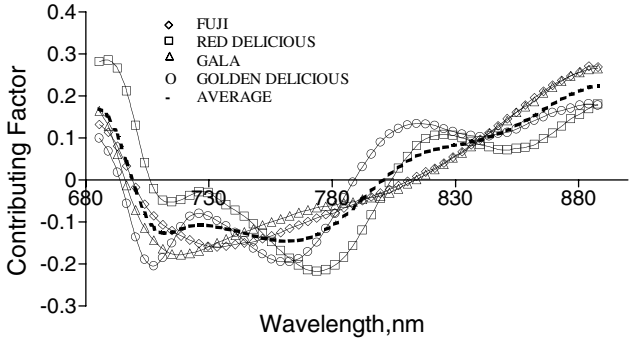

Fig. 7. Spectral range contributions for the four apple cultivars and average contributions to the third principal component axis.

4. Conclusions

A new hyperspectral instrumentation system combining imaging and reflectance spectroscopy has been developed to support the search for new rapid detection systems based on multispectral imaging techniques. A high spatial resolution between 0.5 and 1 mm has been achieved, allowing good spectral and imaging analysis. A higher spectral resolution is also available when using 1 binning along the spectral line but was not necessary for this experiment.

The use of the red chlorophyll absorption band by itself was found to be generally insufficient for good separation of defective/contaminated areas from normal areas. Variations in chlorophyll content between different apples within the same cultivars result in different intensities. Also, the intrinsic variations and/or degradation of chlorophyll or carotenoid with storage and detection conditions could strongly affect a threshold type of analysis. Monochromatic images can therefore be used only for specific contaminations but not for general safety detection purposes.

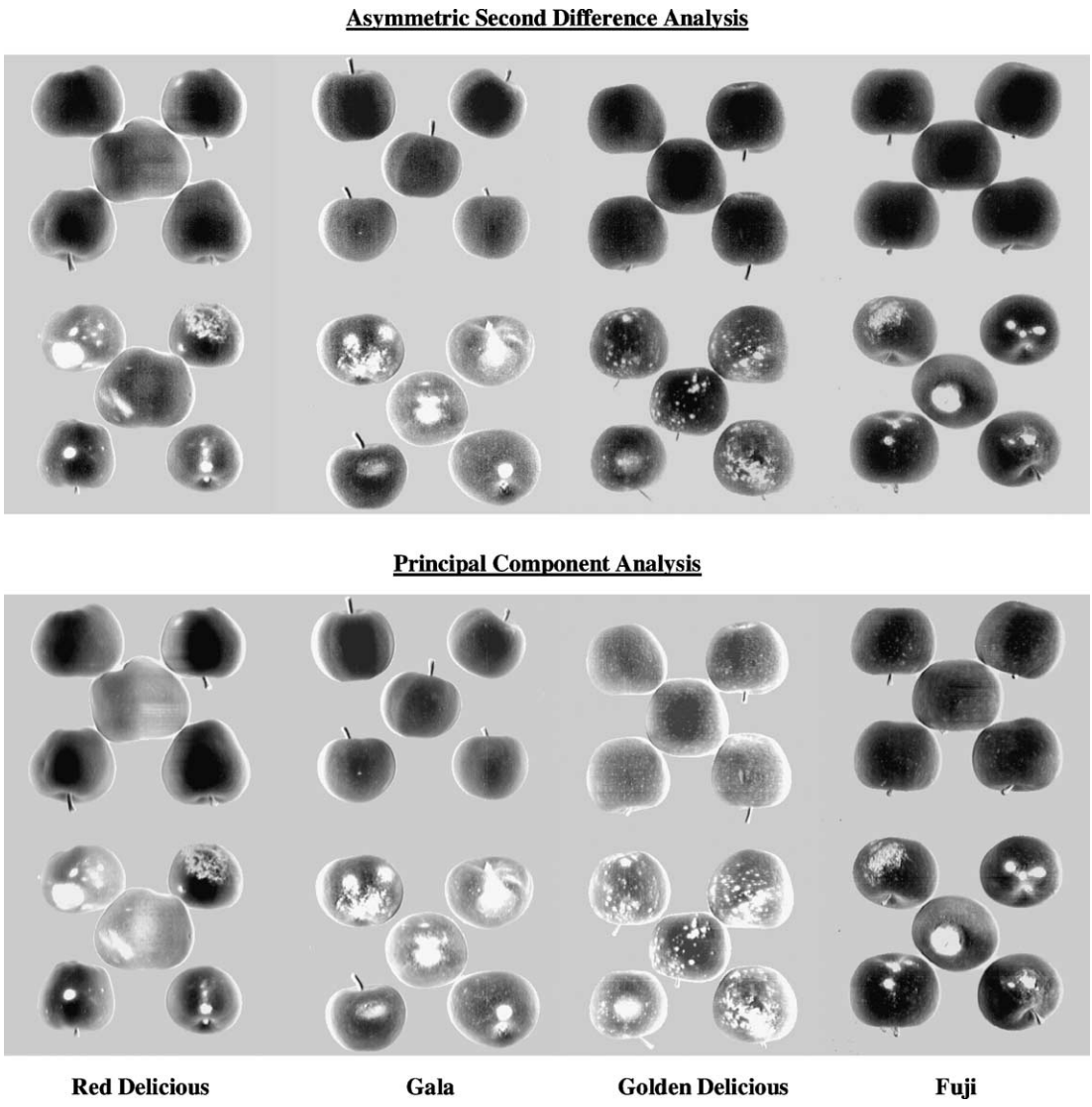

Fig. 8. Comparison of the asymmetric second difference images and the third principal component images for the four apple cultivars. The parameters used for the asymmetric second difference are $\lambda_n = 726$ nm, $g_1 = 11$ and $g_2 = 44$ for Eq. (2).

The asymmetric second difference method is a new analytical technique that has been developed to separate defects/contaminations on different apple cultivars. This method offers a wider use of the spectrum and enhances the symmetrical second differences method. Bruises that were previously difficult to dissociate from normal apple parts become clearly separated. Several advantages exist with this asymmetric second difference method: (1) it is not dependent on the specific apple cultivar; (2) it is simple enough that no multivariate analysis method such as PCA is needed; and (3) it is rapid since only three wavelengths are used. A more complex set with additional wavelengths could be used to optimize the methodology, but this generalization will be detailed in the future. A less complex instrumentation will be developed towards an on-line processing tool using multispectral imaging technology. Rapid data processing with in-house developed algorithms will test and determine the capability and efficiency of this newly developed methodology.

A direct comparison of these second difference methods with principal component analysis shows that the results are very similar in essence. As expected from PCA using the 682–900 nm spectral region, well-defined bruises and also diseased and contaminated areas are observed for the four apple cultivars. However, only the third band of the principal component analysis was utilized due to the more extended variations of the fourth band depending on the apple cultivar, contrary to the previous report (Lu, Chen, Park, & Choi, 1999). This study shows that the asymmetric second difference method and PCA give very similar results for the detection of disease, fungal contamination, bruises, and soil contamination on apples. However, PCA is complex

to use. It requires more data processing time, while the asymmetric second difference method requires only three wavelengths and much less computation time to process the images. Consequently, the asymmetric second difference method can be easily implemented in a three-band multispectral imaging system.

Acknowledgements

The authors would like to thank the Rice Fruit Company, Pennsylvania, for providing access to their fields and production barrels for the apple samplings. We also present our gratitude to Dr. W.R. Hruschka for revising the manuscript.

References

Abbott, J. A., Lu, R., Upchurch, B. L., & Stroshine, R. L. (1997). Technologies for non-destructive quality evaluation of fruits and vegetables. *Horticultural Reviews, 20*, 1–120.

Amanatidou, A., Smid, E. J., & Gorris, L. G. M. (1999). Effect of elevated oxygen and carbon dioxide on the surface growth of vegetable-associated micro-organisms. *Journal of Applied Microbiology, 86*(3), 429–438.

Aneshansley, D. J., Upchurch, B. L., & Throop, J. A. (1997). Reflectance spectra of surface defects on apples. In *Proceedings of the Sensors for Nondestructive Testing International Conference*, Northeast Regional Agricultural Engineering Service, Orlando, FL.

Bergogne-Berezin, E., Courvalin, P., Gehanno, P., Demaresy, J., Perronne, C., & Ducluzeau, R. (1998). Forum on bacterial resistance. *Presse Medicale, 27*(35), 1796–1800.

CDC (1996). Outbreak of *Escherichia coli* 0157:H7 infections associated with drinking unpasteurized commercial apple juice—British Columbia, California, Colorado, and Washington, October 1996. *Morbidity and Mortality Weekly Report*, 45, 975.

CDC (1997). Outbreaks of *Escherichia coli* 0157:H7 infection and cryptosporidiosis associated with drinking unpasteurized apple cider—Connecticut and New York, October 1996. *Morbidity and Mortality Weekly Report*, 46, 4–8.

CDC (1998). Preventing emerging infections diseases: a strategy for the 21st Century, overview of the updated CDC plan. *Morbidity and Mortality Weekly Report*, 47, 1–14.

Chen, Y. R. (1992). Classifying diseased poultry carcasses by visible and near-IR reflectance spectroscopy. *Proceedings of SPIE: Optics in Agriculture and Forestry, 1836*, 46–55.

Chen, Y. R., Park, B., Huffman, R. W., & Nguyen, M. (1998). Classification of on-line poultry carcasses with backpropagation neural networks. *Journal of Food Process Engineering, 21*(1), 33–48.

Cody, S. H., Abbott, S. L., Marfin, A. A., Schulz, B., Wagner, P., Robbins, K., Mohle-Boetani, J. C., & Vugia, D. J. (1999). Two outbreaks of multidrug-resistant *Salmonella* serotype typhimurium DT104 infections linked to raw-milk cheese in Northern California. *Journal of the American Medical Association, 281*, 1805–1810.

Garey, J., & Wolff, M. S. (1998). Estrogenic and anti-progestagenic activities of pyrethroid insecticides. *Biochemical and Biophysical Research Communications, 25*(3), 855–859.

Gat, N. (1998). Real-time multi- and hyper-spectral imaging for remote sensing and machine vision: an overview. ASAE Paper No. 983027, ASAE, St. Joseph, MI.

Govindjee, G., Papageorgiou, G., & Rabinowitch, E. (1967). Chlorophyll fluorescence and photosynthesis. In G. G. Guibault (Ed.), *Fluorescence. Theory, instrumentation, and practice* (pp. 511–564). New York: Marcel Dekker.

Hruschka, W. R. (1987). Data analysis: wavelength selection methods. In P. C. Williams, & K. H. Norris (Eds.), *Near-infrared technology in the agricultural and food industries* (pp. 35–55). St. Paul, MN: AACC.

Kim, M. S., Chen, Y. R., & Mehl, P. M. (2001). Hyperspectral reflectance and fluorescence imaging system for food safety and quality. *Transactions of the ASAE, 44*(3), 721–729.

Liao, K., Reid, J. F., Paulsen, M. R., & Ni, B. (1992). Knowledge-based color discrimination of corn kernels. ASAE Paper No. 923579. ASAE, St. Joseph, MI.

Lu, R., & Chen, Y. R. (1998). Hyperspectral imaging for safety inspection of food and agricultural products. *Proceedings of SPIE: Pathogen Detection and Remediation for Safe Eating, 3544*, 121–133.

Lu, R., Chen, Y. R., Park, B., & Choi, K. H. (1999). Hyperspectral imaging for detecting bruises in apples. ASAE Paper No. 993120. ASAE, St. Joseph, MI.

Malinowski, E. R., & Howery, D. G. (1980). *Factor analysis in chemistry*. New York: J. Wiley & Sons.

Martinsen, P., Schaare, P., & Andrews, M. (1999). A versatile near infrared imaging spectrometer. *Journal of Near Infrared Spectroscopy, 7*(1), 17–25.

Osborne, B. G., Fearn, T., & Hindle, P. H. (1993). *Practical NIR spectroscopy with applications in food and beverage analysis*. Harlow, England: Longman Scientific & Technical.

Park, B., Chen, Y. R., & Nguyen, M. (1998). Multi-spectral image analysis using neural network algorithm for inspection of poultry carcasses. *Journal of Agricultural Engineering Research, 69*(4), 351–363.

Richards, J. A. (1994). *Remote sensing digital image analysis: an introduction*. New York: Springer-Verlag.

Swatland, H. J. (1995). *On-line evaluation of meat*. Lancaster, PA: Technomic Publishing Company, Inc.

Upchurch, B. L., Affeldt, H. A., Hruschka, W. R., Norris, K. H., & Throop, J. A. (1990). Spectrophotometric study of bruises on whole, 'Red Delicious' apples. *Transactions of the ASAE, 33*(2), 585–589.

Williams, P. C., & Norris, K. H. (1987). *Near-infrared technology in the agricultural and food industries*. St. Paul, MN: AACC.